

Review

Constraints of Using Conductive Screen-Printing for Chipless RFID Tags with Enhanced RCS Response

Milan Svanda ^{*}, Jan Machac  and Milan Polivka 

Department of Electromagnetic Field, Faculty of Electrical Engineering, Czech Technical University in Prague, Technická 2, 166 27 Prague, Czech Republic

* Correspondence: svanda.milan@fel.cvut.cz

Abstract: The analysis and experimental verification of the properties of four types of chipless RFID tags with an increased RCS response level designed and fabricated by conductive screen-printing using silver paste on foil and paper substrates was performed. The analytical formula for the quality factor of microstrip structures with a reduced conductivity of the metal layers was used to predict the changes and detectability of the backscattered RCS response. The analysis provides insight into the limitations and outlines the possibilities of chipless structures screen-printed on foil and paper substrates, which can be of significant benefit to further reducing the cost, and to speed up the production of these tags for identification and sensing purposes.

Keywords: chipless RFID; radar cross-section; screen-printing; sensors; symmetry structure

1. Introduction

Radiofrequency identification technology (RFID) is widely used in a variety of applications, primarily in logistics, industry, and health care [1]. The modern Internet of Things paradigm is conditioned by the successful development of this concept mainly for wearable or metal-mountable solutions [2–5], and sensing purposes [6–9].

The relatively high price of the chipped RFID transponders impedes the further expansion of this technology. The chipless RFID [10] as a method of identification information storage without a semiconductor chip represents a promising way of reducing tag costs. The frequency-domain chipless RFID technology represents the most investigated solution, which potentially enables low-cost manufacturing by means of conductive ink printing. The frequency-domain chipless RFID tag is typically composed of an array of mutual detuned scatterers [11–18]. The presence or absence of particular resonant peaks in the RCS response represent the logical one or zero, respectively.

The description of a frequency-domain chipless transponder's behavior can be performed by two fundamental quantities, dependent on the ka product. The radar cross section (RCS) level is the first one, and the quality factor Q determined by a 3 dB bandwidth of resonance peaks or drops is the second one.

The power received at a potential reader of a chipless RFID transponder is directly proportional to the level of the RCS response, and is also inversely proportional to the distance of the reader from the transponder to be identified. Based on this fact, it is reasonable to expect that there will be a specific distance from which the lowest of the resonant peaks/drops of the RCS response will no longer be readable, leading to a fatal decrease in the readability of the entire tag.

On the other hand, the quality factor Q is a crucial parameter of the chipless transponder resonators with respect to the spectral bit capacity. Given the above, we require the narrowest possible bandwidth per transponder resonator for frequency-domain chipless RFID. In other words, we require that the quality factor along with the overall RCS response level be as large as possible. This is a new perspective with respect to conventional antenna



Citation: Svanda, M.; Machac, J.; Polivka, M. Constraints of Using Conductive Screen-Printing for Chipless RFID Tags with Enhanced RCS Response. *Appl. Sci.* **2023**, *13*, 148. <https://doi.org/10.3390/app13010148>

Academic Editors: Ryan Gibson and Hadi Larijani

Received: 2 November 2022

Revised: 15 December 2022

Accepted: 21 December 2022

Published: 22 December 2022



Copyright: © 2022 by the authors. Licensee MDPI, Basel, Switzerland. This article is an open access article distributed under the terms and conditions of the Creative Commons Attribution (CC BY) license (<https://creativecommons.org/licenses/by/4.0/>).

applications. Similarly, for sensor tags, the bandwidth of the resonant dips, which is a key parameter for maximizing the resolution of the frequency shift and hence the sensitivity of the sensing structure, has to be reduced accordingly.

The smaller the electrical size ka , the lower the RCS response, and, concurrently, the higher the Q . As a result, the higher spectral bit capacity, though at the expense of limited read range, is reached. The well-balanced trade-off of these parameters enables reliable identification of the chipless RFID tags in real conditions in conjunction with well-established measurement methods [19,20].

The manufacturing of the transponders by a conductive inkjet- or screen-printing technology [21–26] enables a further reduction of the price cost. Screen- and inkjet printing are forms of modern electronic fabrication technology that can bring a low-cost and environmentally friendly alternative to the common etching fabrication process [23,26]. Due to the refinement of various printing materials, various planar radiating structures have been manufactured by screen-printing or inkjet printing on flexible or rigid substrates [23–26]. However, the influence of reducing Q , due to the lower conductivity of screen-printing to the frequency-domain chipless RFID tags properties mentioned above, has to be verified.

In this paper, an analysis and experimental verification of the performance properties of tags with an increased RCS level (as a crucial parameter for identification in real conditions) designed and fabricated by means of conductive screen-printing was performed. This analysis brings insight into the printed chipless structures' limitation, which is an essential contribution to further cost price reduction and accelerating the production of such tags for both identification and sensory purposes.

2. Theoretical Background

The theoretical analysis presented in this section is used to describe a methodology to maximize the quality factor Q for the simplest of the structures investigated below—the planar strip above the infinite ground plane; see Section 3.3. For even more complex structures, it would be very difficult to develop an analytical model, but the behavior here will have comparable tendencies in principle. Designing a structure with the largest possible Q , and at the same time the largest possible resonant peaks/drops in the RCS response, is the way to enable the realization of such a structure using conductive screen-printing, since the use of screen-printing to realize structures introduces a significant degradation in the quality factor, as well as the level of the individual peaks/drops in the RCS response, as can be seen in the following sections.

Quality Factor Based on Coupled-Mode Theory

The phenomenon of a significant increase in the quality factor for this structure can be easily explained by the image principle. The original dipole (strip) and the image ground current have the same amplitude and opposite phases [27]. Consequently, the electromagnetic field distribution promotes energy storage and subsequently the required increase in the quality factor Q [28–32].

As derived in detail in [33], a single grounded scatterer, see Figure 1, which is excited by a plane electromagnetic wave, can be imagined as a resonant cavity that excites the TM_{01} patch mode. The presence of this mode is related to conductivity and dielectric losses due to the dissipation inside the cavity. The mode also causes the radiation of energy in the form of a propagating wave. According to the theory presented in [27], such a structure can be represented by the reflection coefficient at the interface, at the reference plane of the patch/dipole surface (between the resonator structure and the free space) according to the following relation:

$$\Gamma(f) = \frac{\frac{1}{Q_r} - \frac{1}{Q_0} - \frac{2j(f-f_r)}{f_r}}{\frac{1}{Q_r} + \frac{1}{Q_0} + \frac{2j(f-f_r)}{f_r}}, \quad (1)$$

where Q_r is the radiation (external) quality factor, Q_0 is the unloaded quality factor of the patch cavity, and f_r is the resonant frequency. The CAD formula for the space wave radiation quality factor was derived by Jackson [32] as:

$$Q_r = \frac{3}{16} \frac{\epsilon_r}{pc_1} \frac{L_{eff}}{W_{eff}} \frac{\lambda_0}{h}, \tag{2}$$

where ϵ_r is the relative permittivity and p is the ratio of radiated power by the patch to the radiated power by the equivalent dipole with the same dipole moment as the patch. The constant c_1 is expressed in (4), L_{eff} is the patch effective length, and W_{eff} is the patch width. λ_0 represents the free space wavelength, and h is the dipole substrate thickness between the dipole and the metallic plate.

$$p = 1 + \frac{a_2}{10} (kW_{eff})^2 + \frac{3}{560} (a_2^2 + 2a_4) (kW_{eff})^4 + \frac{1}{5} c_2 (kL_{eff})^2 + \frac{1}{70} (kW_{eff})^2 (kL_{eff})^2, \tag{3}$$

where k is the free space wave constant, $a_2 = -0.16605$, $a_4 = 0.00761$, $c_2 = -0.0914153$,

$$c_1 = \frac{1}{n^2} + \frac{2}{5n^4}, \tag{4}$$

and $n = \sqrt{\mu_r \epsilon_r}$ is the index of refraction of the substrate. The unloaded quality factor Q_0 expresses both conductor and dielectric losses of the cavity and is given by [27]

$$Q_0 = \frac{Q_c Q_d}{Q_c + Q_d}, Q_c = h \sqrt{\frac{\omega}{2}} \mu \sigma, \quad Q_d = \frac{1}{\tan \delta} \tag{5}$$

where ω is the angular frequency, μ represents the permeability, and σ is the conductivity of the metal parts, $\tan \delta$ is the loss tangent of the dielectric substrate. The total (i.e., loaded) quality factor Q_t of the cavity can be calculated according to (6). Q_t includes all loss phenomena except the effect of surface waves, the magnitude of which is negligible.

$$\frac{1}{Q_t} = \frac{1}{Q_r} + \frac{1}{Q_c} + \frac{1}{Q_d} \tag{6}$$

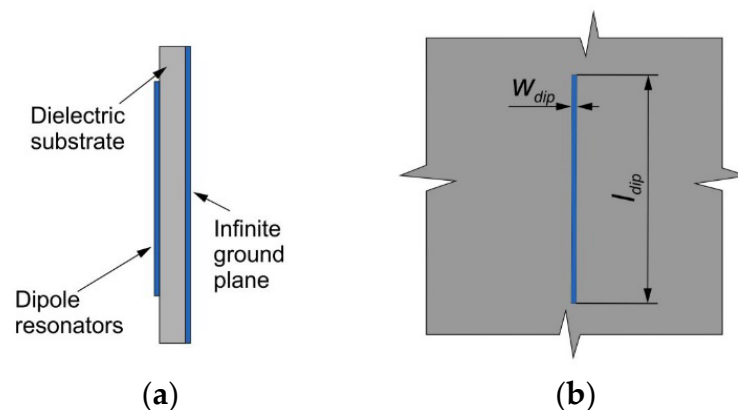


Figure 1. Cross-section (a) and top view (b) of the dipole placed above an infinite metallic plate.

The reflection coefficient at the resonant frequency is derived from (1) as

$$\Gamma(f_r) = \frac{\frac{1}{Q_r} - \frac{1}{Q_0}}{\frac{1}{Q_r} + \frac{1}{Q_0}} \tag{7}$$

Based on this analysis, three different conditions for the coupling of dissipation and leakage modes can be expressed:

- (1) $Q_r > Q_0$, under-coupled,
- (2) $Q_r < Q_0$, over-coupled,
- (3) $Q_r = Q_0$, critically-coupled.

For the case under study, the third condition is of interest, i.e., the critical coupling at which the maximum energy absorption is attained, which consequently leads to the maximum achievable Q for a given geometry. We consider a low-loss foam dielectric substrate with a relative permittivity $\epsilon_r = 1.3$, loss tangent $\tan \delta \sim 10^{-3}$, and two cases of metal conductivity—copper $\sigma = 5.8 \times 10^7$ S/m and screen-printing silver paste $\sigma = 1.6 \times 10^6$ S/m. A dipole of length $L_{\text{dip}} = 46$ mm is situated on a foam substrate of variable thickness h over an infinitely large conductive plane. Figure 2 shows the quality factors of a cavity consisting of 0.2 mm and 1 mm wide dipoles placed above the conducting plane depending on the substrate height h . Surface plots in Figure 3 depict the dependence of the reflection coefficient on frequency along with the distance of the dipole from the conducting plane.

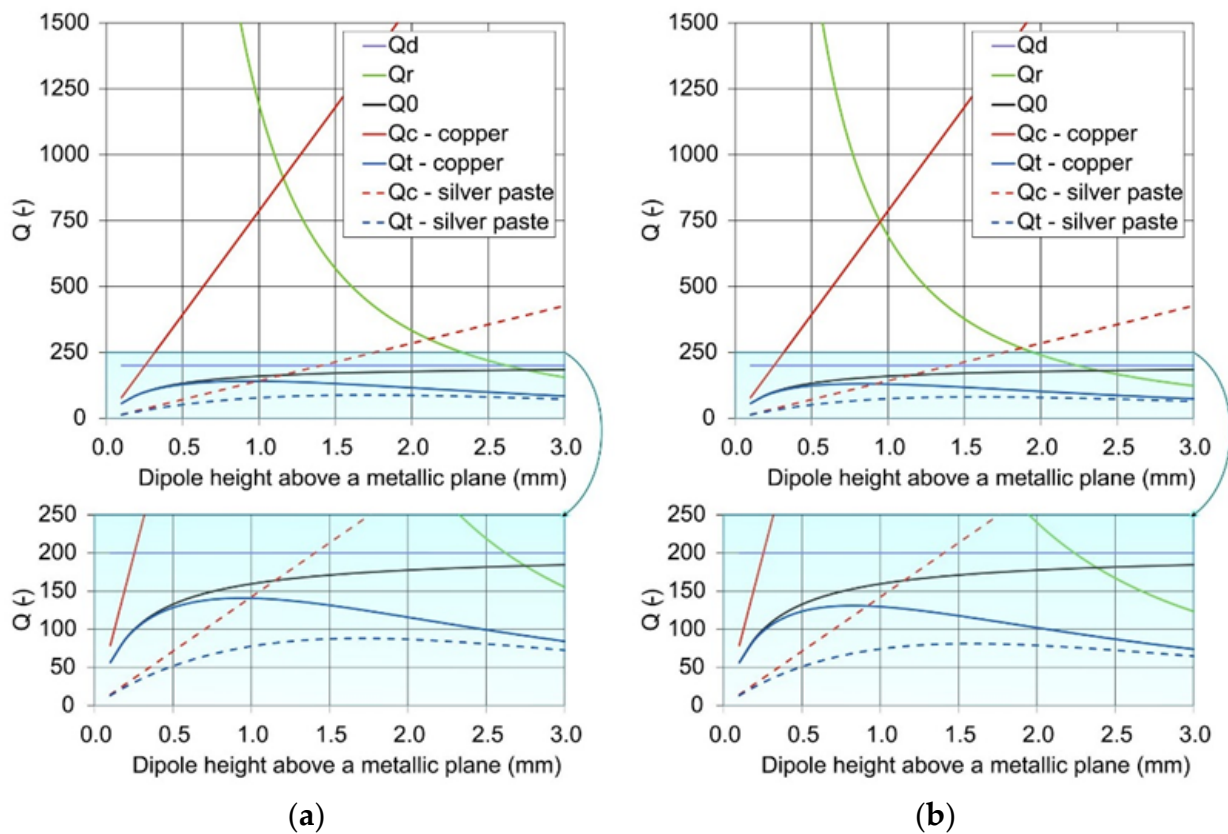


Figure 2. Quality factors vs. height of (a) a narrow dipole $46 \times 0.2 \text{ mm}^2$ and (b) a wide dipole $46 \times 1 \text{ mm}^2$ situated on a foam substrate above an infinite metallic plane for conductivity of copper (5.8×10^7 S/m) and silver paste (1.6×10^6 S/m). Intersection of the Q_0 and Q_r curves correspond to critical coupling and deep resonant minima on the RCS curve.

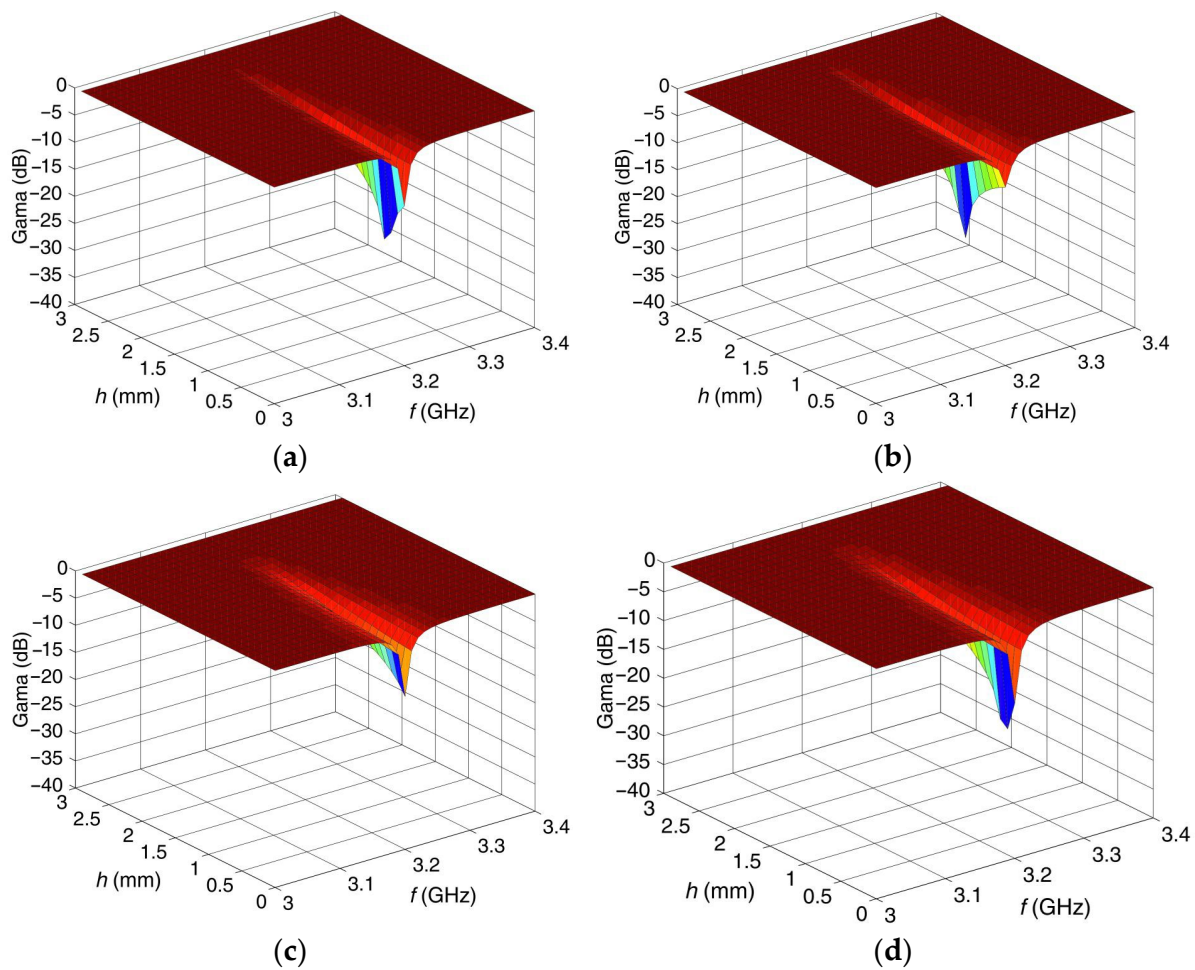


Figure 3. Reflection coefficient vs. frequency and dipole height of a dipole situated on a foam substrate above an infinite metallic plane. (a) Narrow dipole $46 \times 0.2 \text{ mm}^2$, copper; (b) wide dipole $46 \times 1 \text{ mm}^2$, copper; (c) narrow dipole $46 \times 0.2 \text{ mm}^2$, silver paste; (d) wide dipole $46 \times 1 \text{ mm}^2$, silver paste.

From Figure 2, it can be said that there is an optimal dipole height for achieving critical coupling, and hence maximizing the total quality factor Q_t . This height ranges from 0.5 mm to 1.2 mm for both dipole widths investigated with copper metallization. Through the use of the screen-printing silver paste metallization, the optimal height is noticeably shifted, and it ranges from 1.2 mm to 2.0 mm for both dipole widths. In addition, the narrowing of the dipole width applies the reflection coefficient degradation, as can be seen in Figure 3. Furthermore, it is worth noting that the increase in permittivity and losses in the substrate lead to the requirement of a larger distance of the dipole from the conducting plane in order to achieve critical coupling ($Q_r = Q_0$). A detailed study about this effect can be found in [33].

Due to the reduction of the conductivity of the silver paste compared to the copper, the value of the reflection coefficient degrades; see the comparison of Figure 3a,b with Figure 3c,d. A similar effect can be observed when the dipole width is narrowed; see comparison of Figure 3a,c with Figure 3b,d.

Based on these results, a height of $h = 1 \text{ mm}$, which is the closest available foam substrate height, was chosen for implementing the geometry from Section 3.3 for both the standard “copper on substrate” as well as screen-printing samples to the desired value from Figures 2 and 3.

3. Tags with Enhanced RCS Response

The main issue of the design of the chipless RFID transponders (for identification as well as sensing) is ensuring a sufficiently high radar cross-section (RCS) to detect the tag at a sufficient distance [13]. The second important issue is to ensure the proper operation of the tag in any surroundings. This means even in the close presence of metallic or loss dielectric objects, especially, that create relatively strong unwanted reflections and thus mask the desired response [19]. Three chipless RFID transponders based on different approaches to the RCS response level enhancement that enables the reduction of false reflections developed by the authors were analyzed from the screen-printing point of view [33–35]. These structures were compared with the improved re-arranged U-dipole structure with very good robustness of the RCS response [13]. As for the transponders used for encoding multi-bit information, 20-bit versions were chosen. This is a suitable compromise between the number of bits needed to encode the information and the area occupied by such a structure (space bit density). The number of bits can be arbitrary with respect to a particular application.

All tags were re-designed for a Folex Folanorm (polyester film) dielectric substrate ($\epsilon_r = 4$, $\tan \delta = 0.005$) with a thickness of 125 μm . The screen-printing of the conductive parts was performed by ESL Electroscience polymer silver conductor paste ESL 1901-S with resistivity 20 $\text{m}\Omega/\text{sq}$ and thickness 30 μm ; for details, see in Section 4. The size of all the structures are summarized in Tables 1–4, respectively.

Table 1. Dimensions of shorted re-arranged U-dipole.

l_{tag} (mm)	w_{tag} (mm)	l_{dip} (mm)	g_{dip} (mm)	s_{dip} (mm)	w_{strip} (mm)
35	75	14.8 to 24.3	1	0.5	1

Table 2. Dimensions of U-Slots in the metallic plate.

l_{tag} (mm)	w_{tag} (mm)	l_{slot} (mm)	g_{slot} (mm)	s_{slot} (mm)	w_{slot} (mm)
52	50	13 to 22.5	0.5	0.25	1.5

Table 3. Dimensions of dipoles over metallic plate.

l_{tag} (mm)	w_{tag} (mm)	l_{dip} (mm)	g_{dip} (mm)	w_{dip} (mm)
60	60	31.5 to 50.5	1.5	1

Table 4. Size of IC U-dipole coupled in the metallic loop.

l_{tag} (mm)	w_{tag} (mm)	l_{loop} (mm)	w_{loop} (mm)	w_{strip} (mm)	$l_{\text{U-dip}}$ (mm)
50	32	40	25	5	5.3
$w_{\text{U-dip}}$ (mm)	w_{ID} (mm)	$g_{\text{U-dip}}$ (mm)	g_{ID} (mm)	g_{coupling} (mm)	N (-)
0.5	0.2	3.4	0.25	2	7

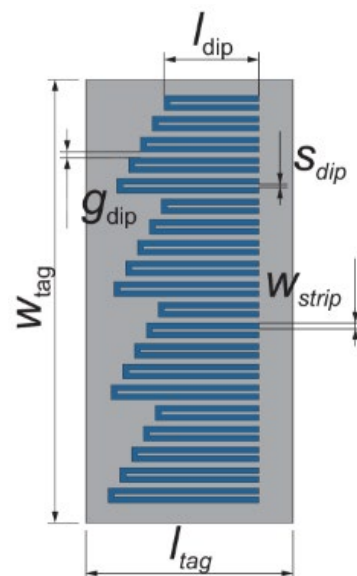
The analysed tags were simulated by MoM software Zeland IE3D. The performance comparison of the tags can be seen in Table 5.

Table 5. Performance comparison of frequency-domain chipless RFID tags.

Resonator Type [Reference]	Frequency Range (GHz)	Number of Bits	Spatial Density at Center Freq. (bit/ λ^2)	Spectral Capacity (bit/GHz)	Encoding Capacity (bit/ λ^2 /GHz)	RCS (dBsm)	Platform Tolerance	Number of Metallic Layers	Peak Depth—DPS Technology (dB)	Peak Depth—Screen-Printing (dB)	Peak Depth Screen-Print./DPS Ratio (dB)
Re-arranged shorted U-dipoles [13]	2.2–3.8	20	112.0	12.5	70.0	−35	No	1	4	-	-
Re-arranged U-slots in the metallic plate [34]	2.2–3.8	20	76.9	12.5	48.1	−17	No	1	1	-	-
Array of detuned planar dipoles closely coupled to a rectangular metallic plate [33]	2.2–3.5	20	61.6	15.4	47.4	−15	Yes	2	2	0.5	−1.5
Interdigital U-dipole coupled to the metallic loop sensor tag [35]	2.6–3.6	1	5.3	-	-	−17	No	1	17	4	−13

3.1. Re-Arranged Shorted U-Dipoles

As shown in Figure 4, the geometry of the first 20-bit chipless RFID tags is composed of an array of U-shaped shorted strip scatterers. The geometry of the basic element is inspired by the structure used in [11]. To improve the robustness of the RCS response, the mutual coupling between scatterers with neighbouring resonance frequencies was reduced by the element re-arrangement proposed in [13].

**Figure 4.** Sketch of 20-bit shorted re-arranged U-dipole tag.

The size of the tag can be seen in Table 1. The incident excitation field is oriented vertically to the tag presented in Figure 4. The simulated RCS response of the tag is depicted in Figure 5.

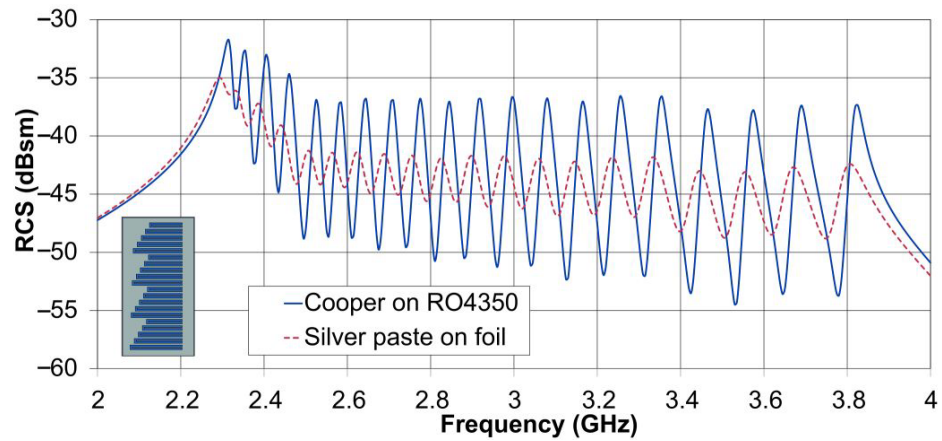


Figure 5. Simulated RCS of shorted re-arranged U-dipole tag.

3.2. Re-Arranged U-Slots in the Metallic Plate

The tag depicted in Figure 6 represents the first type of RCS response enhancement, based on a metallic rectangular plate which provides a monotonous RCS response over the frequency band used with a level higher than -20 dBsm [34]. The resonating elements are formed by shorted coplanar U-slots introduced into the rectangle. The electric field vector, which excites the electric field in the short middle part of the slot, is oriented vertically to the tag presented in Figure 6. The simulated RCS response can be seen in Figure 7.

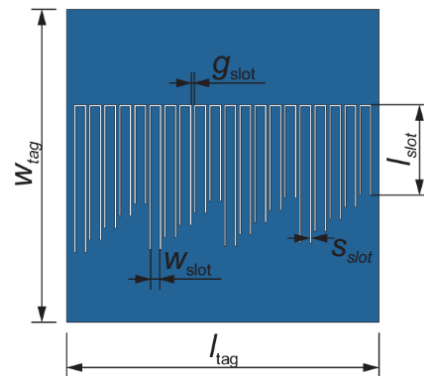


Figure 6. Sketch of 20-bit re-arranged U-slots in the metallic plate tag.

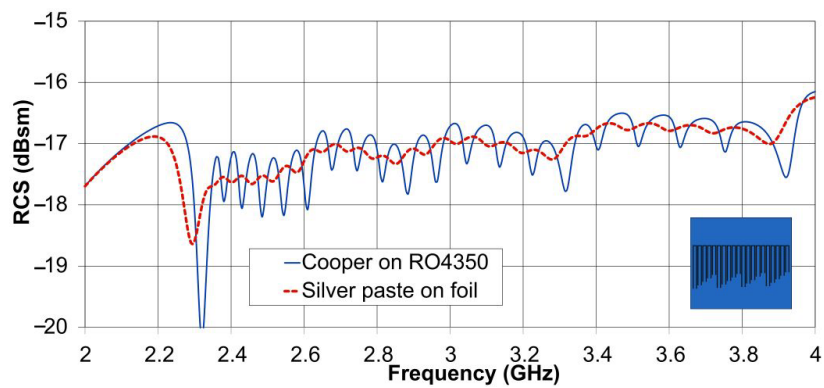


Figure 7. Simulated RCS of re-arranged U-slots in the metallic plate tag.

3.3. Array of Detuned Planar Dipoles Closely Coupled to a Rectangular Metallic Plate

The second type of RCS response enhancement is based on an array of detuned planar dipoles closely coupled to a rectangular metallic plate; see Figure 8. The monotonous RCS response is reached by the rectangular plate, whereas the resonance drops are caused by the detuned dipoles situated on the substrate whose thickness is 1.1 mm. The substrate comprises of the Folanorm polyester film and a foam layer. The relative permittivity of the film is $\epsilon_r = 4$, the loss tangent is $\tan \delta = 0.005$, and the thickness is 0.3 mm, while the relative permittivity is $\epsilon_r \sim 1.3$, the loss tangent is $\tan \delta \sim 0.02$, and the thickness is 1 mm. These properties enable the effective permittivity reduction and, consequently, they enable the deepening of the resonant drops [33]. The simulated RCS response is depicted in Figure 9.

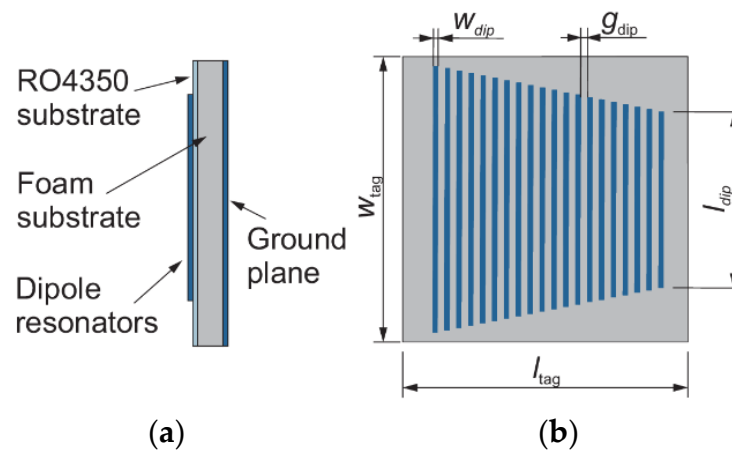


Figure 8. Cross-section (a) and top view (b) of the detuned dipoles array placed above a metallic plate chipless RFID tag.

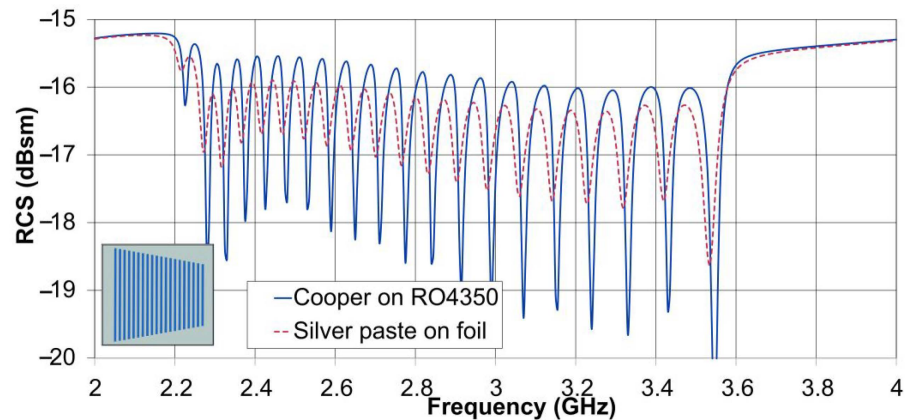


Figure 9. Simulated RCS of the array of detuned planar dipoles closely coupled to a rectangular metallic plate.

3.4. Interdigital U-Dipole Coupled to the Metallic Loop

The IC U-dipole resonator coupled in the metallic loop represents the third attempt of the RCS enhancement; see Figure 10. The presented geometry with one resonator is designed for chipless RFID sensor applications, where the space bit density is not the main requirement [35,36]. The number of loading interdigital fingers of the folded U-dipole changes the loading capacitance, and consequently the resonant frequency.

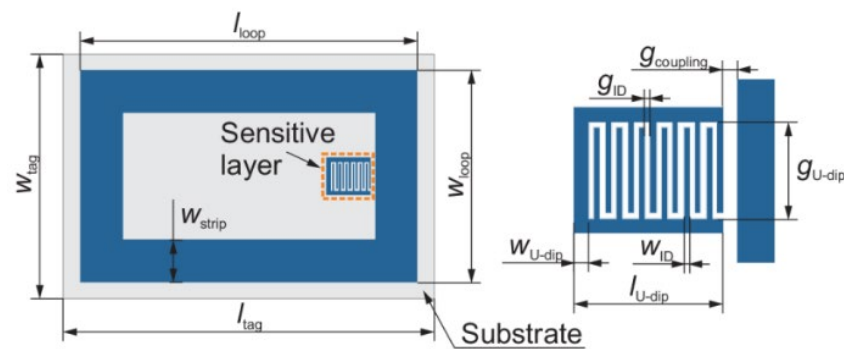


Figure 10. Sketch of IC U-dipole coupled in the metallic loop sensor tag.

This effect can be applied in a sensor at which the detected quantity (e.g., by means of a sensitive layer situated on top of the resonator) can change the value of the capacitor loading the folded dipole. The simulated RCS response of one-bit chipless sensor tag is depicted in Figure 11.

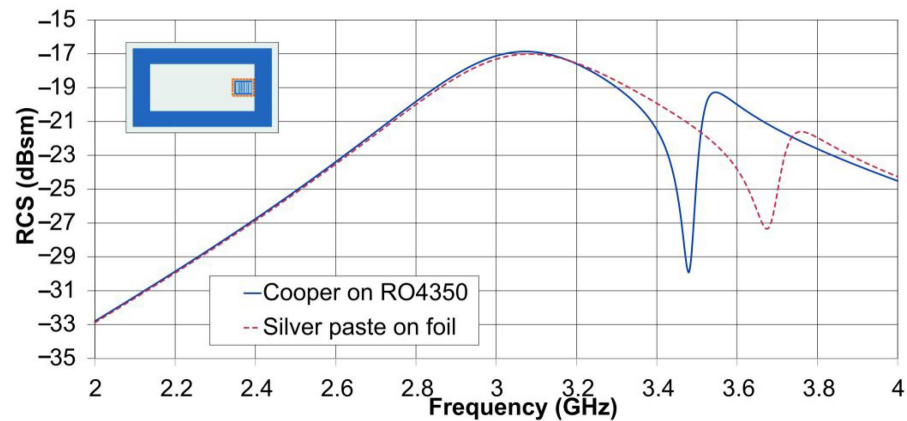


Figure 11. Simulated RCS of IC U-dipole coupled in the metallic loop sensor tag.

4. Conductive Screen-Printing of the Tags with Enhanced RCS Response

As mentioned above, all tags were re-designed for a Folanorm polyester film dielectric substrate with relative permittivity $\epsilon_r = 4$, $\tan \delta = 0.005$, and with the thickness of 125 μm . The same geometry without size optimization was printed on a standard 200 g/m^2 quarto paper substrate with thickness 100 μm , relative permittivity $\epsilon_r = 2.2$, and $\tan \delta = 0.03$. A comparison of the measured results can be seen in Section 5.

The screen-printing of the conductive parts was performed by ESL Electroscience polymer silver conductor paste ESL 1901-S with thickness 30 μm . An Aurel C880 (Aurel s.p.a., Modigliana, Italy), a semi-automatic printer, was used. After screen-printing and curing, the silver conductor remains reasonably flexible and the resistance of the conductor remains constant over time. The paste resistivity is lower than 20 $\text{m}\Omega/\text{sq}$ measured on a 100 $\text{mm} \times 0.25 \text{ mm}$ conductor track. In order to ensure a sufficient quality of the metallic surfaces, screen-printing of the conductive paste was repeated three times. The paste was then cured at a temperature of 80 $^\circ\text{C}$ for 30 min.

5. Measurement

The simulated results of the common substrate manufactured as well as the conductive printed transponders were verified by the monostatic measurement of the RCS response in an anechoic chamber; see Figure 12.

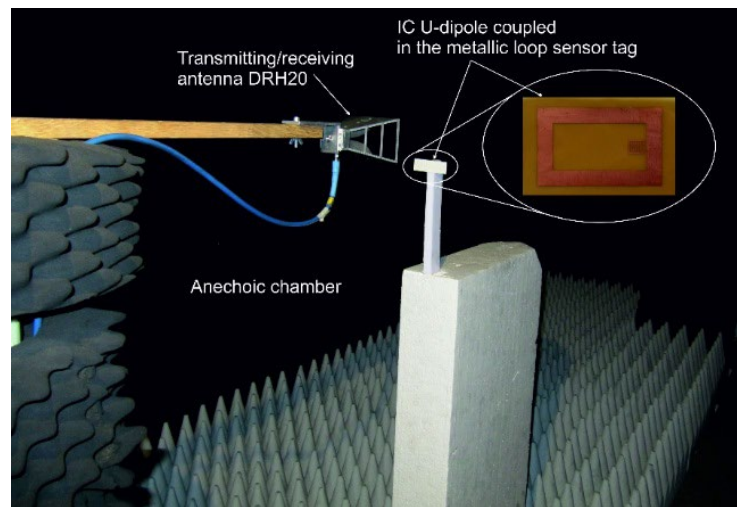


Figure 12. Monostatic measurement setup in anechoic chamber with detail of IC U-dipole coupled in the metallic loop sensor tag.

The double ridge horn antenna DRH 20 [37] was used for measurement because of the reflection coefficient from which the resulting RCS response was evaluated with the help of the one-port Formula (8). The measured transponders were situated at a distance of 500 mm in front of the antenna. The RCS response of the tag was calculated using relations given by [33] as

$$\sigma^{tag} = 20 \log \left| \frac{S_{11}^{tag} - S_{11}^{iso}}{S_{11}^{ref} - S_{11}^{iso}} \right| \sigma^{ref}, \quad (8)$$

where S_{11}^{tag} is the reflection coefficient when the measured tag is used as a scatterer. In turn, S_{11}^{ref} symbolizes the reflection coefficient when a reference metallic plate is used as a scatterer. Next, S_{11}^{iso} represents the reflection coefficient of the antenna itself when no scatterer is installed and comprises residual reflection from the experiment environment. Finally, σ^{tag} is the RCS of the measured tag, while σ^{ref} is the RCS of the reference scatterer, which is a rectangular metal plate with the dimensions of $a \times b = 60 \times 60 \text{ mm}^2$ and a thickness of 0.3 mm. The analytical formula for the reference scatterer RCS is given by [35] as

$$\sigma^{ref} = 4\pi \frac{a^2 b^2}{\lambda^2}, \quad (9)$$

where λ is the signal wavelength in free space.

The measured RCS of the above-presented structures manufactured by screen-printing on Folanorm polyester film and paper substrate compared to the standard copper-on-microwave substrate technology is depicted in Figures 13–16. It can be seen that in the case of a large array of resonators, the individual resonance drops are degraded; however, in the case of a small number of bits (e.g., in the case of sensor transponders; see Figure 16), this degradation is still readable and acceptable for the specific purpose. The frequency shift of the peaks/drops in comparison with the “copper on substrate” realization is caused by the effective permittivity difference. The screen-printed versions of the tags have unchanged dimensions and the geometry of the motif.

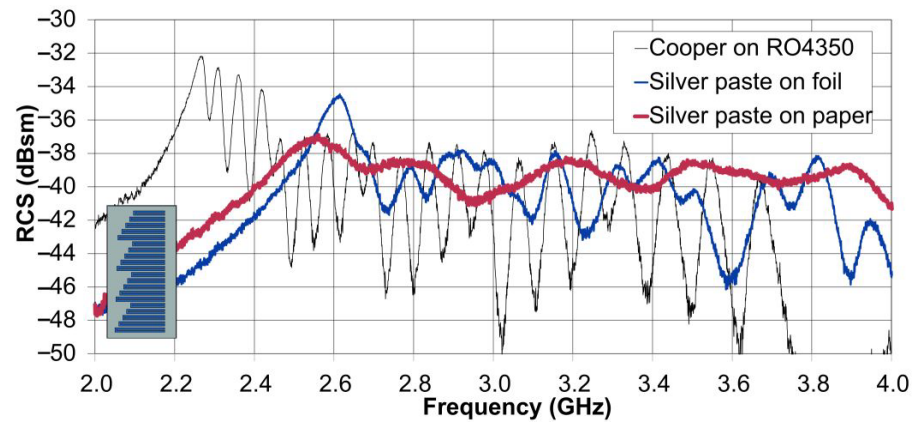


Figure 13. Measured RCS of shorted re-arranged U-dipole tag manufactured by the screen-printing technology on Folanorm polyester film and a paper substrate compared to a standard copper-on-microwave substrate technology.

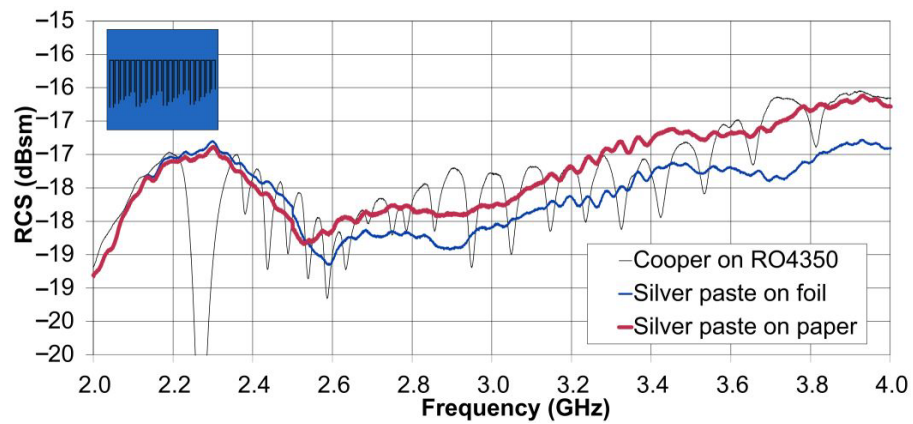


Figure 14. Measured RCS of re-arranged U-slots in the metallic plate tag manufactured by the screen-printing technology on Folanorm polyester film and a paper substrate compared to a standard copper-on-microwave substrate technology.

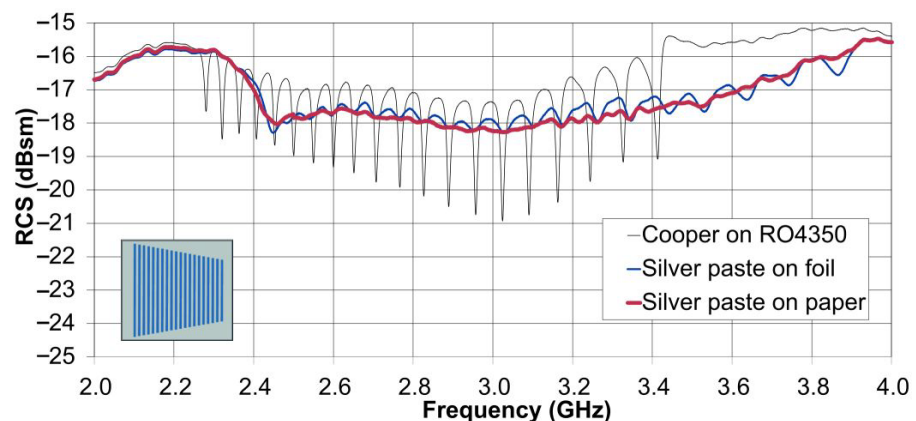


Figure 15. Measured RCS of an array of detuned planar dipoles closely coupled to a rectangular metallic plate manufactured by the screen-printing technology on Folanorm polyester film and a paper substrate compared to a standard copper-on-microwave substrate technology.

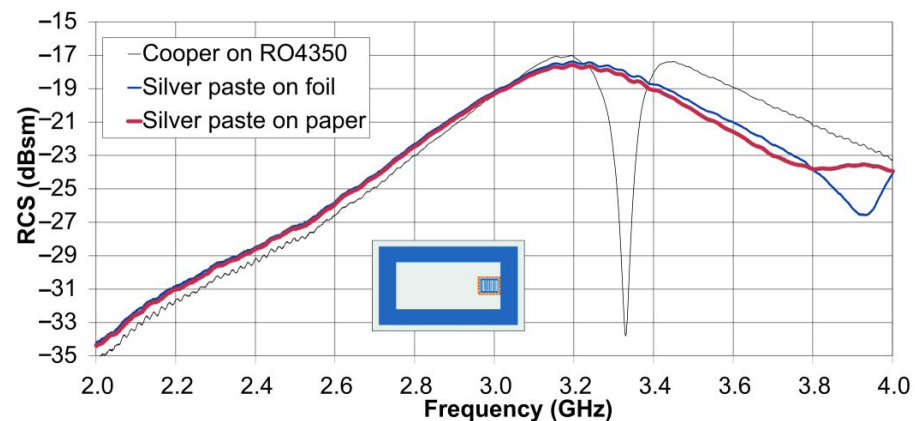


Figure 16. Measured RCS of IC U-dipole coupled in the metallic loop sensor tag manufactured by the screen-printing technology on Folanorm polyester film and a paper substrate compared to a standard copper-on-microwave substrate technology.

6. Conclusions

Chipless RFID transponders, based on different types of elements with an enhanced RCS response, developed by the authors were analyzed in terms of the application of screen-printing technology using silver paste with reduced conductivity, and foil and paper substrates. The reduced conductivity of the metallic layers reduces the quality factor of the individual resonators, and thus degrades the parameters and the readability of the resonance minima on the RCS response curve compared to the conventional copper-clad woven-glass laminate technology. It can be concluded that, in order to realize resonant reflective structures by screen printing using silver paste, it is crucial to ensure deep resonant dips. The relative deterioration of the RCS response of scatterers may only be acceptable at high RCS levels with deep resonant dips, especially when using sensor transponders with a small number of bits.

Author Contributions: Conceptualization, M.S., J.M. and M.P.; methodology, M.S. and J.M.; validation, M.S. and M.P.; formal analysis, M.P.; investigation, M.S., J.M. and M.P.; resources, M.S.; data curation, M.S.; writing—original draft preparation, M.S.; writing—review and editing, M.S.; visualization, M.S.; supervision, J.M. and M.P.; project administration, M.S.; funding acquisition, M.S. All authors have read and agreed to the published version of the manuscript.

Funding: This work was funded by the Ministry of Education, Youth and Sports of the Czech Republic (program: INTER-EXCELLENCE; subprogram: INTER-COST; project: LTC20012) and the COST—European Cooperation in Science and Technology (COST Action CA18223 SyMat).

Institutional Review Board Statement: Not applicable.

Informed Consent Statement: Not applicable.

Data Availability Statement: The data presented in this study are available in the article figures and tables.

Acknowledgments: The authors thank Jan Prasek from the Department of Microelectronics, Faculty of Electrical Engineering and Communication, Brno University of Technology for the screen-printing of the structures.

Conflicts of Interest: The authors declare no conflict of interest.

References

1. Finkenzeller, K. *RFID Handbook: Fundamentals and Applications in Contactless Smart Cards and Identification*, 2nd ed.; John Wiley & Sons: Hoboken, NJ, USA, 2005.
2. Babar, A.A.; Bjorninen, T.; Bhagavati, V.A.; Sydanheimo, L.; Kallio, P.; Ukkonen, L. Small and flexible metal mountable passive UHF RFID tag on high-dielectric polymer-ceramic composite substrate. *IEEE Antennas Wirel. Propag. Lett.* **2012**, *11*, 1319–1322. [[CrossRef](#)]

3. Marrocco, G. RFID antennas for the UHF remote monitoring of human subjects. *IEEE Trans. Antennas Propag.* **2007**, *55*, 1862–1870. [[CrossRef](#)]
4. Svanda, M.; Polivka, M. Two novel extremely low-profile slot-couplet two-element patch antennas for UHF RFID of people. *Microw. Opt. Technol. Lett.* **2010**, *52*, 249–252. [[CrossRef](#)]
5. Svanda, M.; Polivka, M.; Hudec, P. Novel low-profile foam dielectric over-the-shoulder antenna based on coupled patches technique. *Microw. Opt. Technol. Lett.* **2013**, *55*, 593–597. [[CrossRef](#)]
6. Occhiuzzi, C.; Caizzone, S.; Marrocco, G. Passive UHF RFID antennas for sensing applications: Principles, methods and classifications. *IEEE Antennas Propag. Mag.* **2014**, *55*, 14–34. [[CrossRef](#)]
7. Kracek, J.; Švanda, M.; Mazanek, M.; Machac, J. Implantable semi-active UHF RFID tag with inductive wireless power transfer. *IEEE Antennas Wirel. Propag. Lett.* **2016**, *15*, 1657–1660. [[CrossRef](#)]
8. Carvalho, N.B.; Georgiadis, A.; Costanzo, A.; Stevens, N.; Kracek, J.; Pessoa, L.M.; Roselli, L.; Dualibe, F.; Schreurs, D.; Mutlu, S.; et al. Europe and the Future for WPT COST Action IC1301 Team. *IEEE Microw. Mag.* **2017**, *18*, 56–87.
9. Occhiuzzi, C. RFID Passive gas sensor integrating carbon nanotubes. *IEEE Trans. Microw. Theory Tech.* **2011**, *59*, 2674–2684. [[CrossRef](#)]
10. Karmakar, N.C. Tag, you're it radar cross section of chipless RFID tags. *IEEE Microw. Mag.* **2016**, *17*, 64–74. [[CrossRef](#)]
11. Vena, A.; Perret, E.; Tedjini, S. A fully printable chipless RFID tag with detuning correction technique. *IEEE Microw. Wirel. Compon. Lett.* **2012**, *22*, 209–211. [[CrossRef](#)]
12. Rance, O.; Siragusa, R.; Lemaitre-Auger, P.; Perret, E. Toward RCS magnitude level coding for chipless RFID. *IEEE Trans. Microw. Theory Tech.* **2016**, *64*, 2315–2325. [[CrossRef](#)]
13. Polivka, M.; Havlicek, J.; Svanda, M.; Machac, J. Improvement in robustness and recognizability of RCS response of U-shaped strip-based chipless RFID tags. *IEEE Antennas Wirel. Propag. Lett.* **2016**, *15*, 2000–2003. [[CrossRef](#)]
14. Polivka, M.; Svanda, M.; Machac, J. Chipless RFID tag with an improved rcs response. In Proceedings of the European Microwave Week 2014 (44th EuMC, EuRAD, EuMIC, EuWT) [CD-ROM], Rome, Italy, 6–9 October 2014.
15. Havlicek, J.; Svanda, M.; Polivka, M.; Machac, J.; Kracek, J. Chipless RFID tag based on electrically small spiral capacitively loaded dipole. *IEEE Antennas Wirel. Propag. Lett.* **2017**, *16*, 3051–3054. [[CrossRef](#)]
16. Huang, H.; Su, L. A compact dual-polarized chipless RFID tag by using nested concentric square loops. *IEEE Antennas Wirel. Propag. Lett.* **2017**, *16*, 1036–1039. [[CrossRef](#)]
17. Added, M.; Boulejeff, N.; Svanda, M.; Ghannouchi, F.M.; Vuong, T.-P. High-Performance chipless radio-frequency identification tags: Using a slow-wave approach for miniaturized structure. *IEEE Antennas Propag. Mag.* **2019**, *61*, 46–54. [[CrossRef](#)]
18. Costa, F.; Genovesi, S.; Monorchio, A. A chipless RFID based on multiresonant high-impedance surfaces. *IEEE Trans. Microw. Theory Tech.* **2013**, *61*, 146–152. [[CrossRef](#)]
19. Kracek, J.; Svanda, M.; Hoffmann, K. Scalar method for reading of chipless rfid tags based on limited ground plane backed dipole resonator array. *IEEE Trans. Microw. Theory Tech.* **2019**, *67*, 4547–4558. [[CrossRef](#)]
20. Genovesi, S.; Costa, F.; Dicandia, F.A.; Borgese, M.; Manara, G. Orientation-insensitive and normalization-free reading chipless rfid system based on circular polarization interrogation. *IEEE Trans. Antennas Propag.* **2020**, *68*, 2370–2378. [[CrossRef](#)]
21. Špůrek, J.; Raida, Z.; Láčák, J.; Mikulášek, T.; Vélím, J.; Prášek, J. Circular slot antenna array printed on 3d textile substrate. *Elektrorevue* **2017**, *19*, 140–144.
22. Yang, L.; Rida, A.; Vyas, R.; Tentzeris, M.M. RFID tag and rf structures on a paper substrate using inkjet-printing technology. *IEEE Trans. Microw. Theory Tech.* **2007**, *55*, 2894–2901. [[CrossRef](#)]
23. Tehrani, B.K.; Cook, B.S.; Tentzeris, M.M. Inkjet printing of multilayer millimeter-wave yagi-uda antennas on flexible substrates. *IEEE Antennas Wirel. Propag. Lett.* **2016**, *15*, 143–146. [[CrossRef](#)]
24. Whittow, W.G.; Chauraya, A.; Vardaxoglou, J.C.; Li, Y.; Torah, R.; Yang, K.; Beeby, S.; Tudor, J. Inkjet-printed microstrip patch antennas realized on textile for wearable applications. *IEEE Antennas Wirel. Propag. Lett.* **2014**, *13*, 71–74. [[CrossRef](#)]
25. Rashidian, A.; Shafai, L.; Sobociński, M.; Peräntie, J.; Juuti, J.; Jantunen, H. Printable planar dielectric antennas. *IEEE Trans. Antennas Propag.* **2016**, *64*, 403–413. [[CrossRef](#)]
26. Sun, H.; Xiao, G.; Lang, S.; Zhang, Z.; Tao, Y. Screen Printed HF RFID Antennas on Polyethylene Terephthalate Film. *IEEE J. Radio Freq. Identif.* **2019**, *3*, 91–97. [[CrossRef](#)]
27. Balanis, C.A. *Antenna Theory, Analysis and Design*, 2nd ed.; John Wiley & Sons, Inc.: New York, NY, USA, 1997.
28. Sten, J.C.E.; Hujanen, A.; Koivisto, P.K. Quality factor of an electrically small antenna radiating close to a conducting plane. *IEEE Trans. Antennas Propag.* **2001**, *49*, 829–837. [[CrossRef](#)]
29. Best, S.R. Improving performance properties of a dipole element closely spaced to a PEC ground plane. *IEEE Antennas Wirel. Propag. Lett.* **2004**, *3*, 359–363. [[CrossRef](#)]
30. Chang, H.C.; Cho, Y.H.; Kwon, D.-H. Radiation Q bounds for small electric dipoles over a conducting ground plane. *IEEE Trans. Antennas Propag.* **2014**, *62*, 2031–2040. [[CrossRef](#)]
31. Hazdra, P.; Capek, M.; Eichler, J.; Mazanek, M. The radiation Q factor of a horizontal $\lambda/2$ dipole above ground plane. *IEEE Antennas Wirel. Propag. Lett.* **2014**, *13*, 1073–1075. [[CrossRef](#)]
32. Jackson, D.R. Microstrip antennas. In *Antenna Engineering Handbook*; Volakis, J.L., Ed.; McGraw Hill: New York, NY, USA, 2007.
33. Svanda, M.; Polivka, M.; Havlicek, J.; Machac, J.; Werner, D.H. Platform tolerant, high encoding capacity dipole array-plate chipless RFID tags. *IEEE Access* **2019**, *7*, 138707–138720. [[CrossRef](#)]

34. Svanda, M.; Polivka, M.; Havlicek, J.; Machac, J. Chipless RFID tag with an improved magnitude and robustness of RCS response. *Microw. Opt. Technol. Lett.* **2017**, *59*, 488–492. [[CrossRef](#)]
35. Svanda, M.; Machac, J.; Polivka, M.; Havlova, S.; Fitl, P.; Vrnata, M. Chipless RFID tag with enhanced RCS used as phthalocyanine chemical gas sensor. *IEEE Antennas Wirel. Propag. Lett.* **2020**, *19*, 1556–1560. [[CrossRef](#)]
36. Ayadi, H.; Machac, J.; Svanda, M.; Boulejfen, N.; Latrach, L. Proof-of-Concept of Reconfigurable Solvent Vapors Sensor Tag with Wireless Power Transfer for IoT Applications. *Appl. Sci.* **2022**, *12*, 10266. [[CrossRef](#)]
37. Model DRH20—Double Ridge Waveguide Horn. RFspin s.r.o. Available online: <http://www.rfspin.cz/en/antennas/drh20.php> (accessed on 10 March 2022).

Disclaimer/Publisher’s Note: The statements, opinions and data contained in all publications are solely those of the individual author(s) and contributor(s) and not of MDPI and/or the editor(s). MDPI and/or the editor(s) disclaim responsibility for any injury to people or property resulting from any ideas, methods, instructions or products referred to in the content.